Soft-x-ray fragmentation studies of molecular ions

Andreas Wolf, Henrik B Pedersen, Lutz Lammich, Brandon Jordon-Thaden, Simon Altevogt, Christian Domesle, Uwe Hergenhahn, Marko Förstel, Oded Heber

Soft-X-ray fragmentation studies of molecular ions

Andreas Wolf[1], Henrik B Pedersen[1,2], Lutz Lammich[2], Brandon Jordon-Thaden[1], Simon Altevogt[1], Christian Domesle[1], Uwe Hergenhahn[3], Marko Förstel[3] and Oded Heber[4]

[1] Max-Planck-Institut für Kernphysik, Saupfercheckweg 1, 69117 Heidelberg, Germany

[2] Department of Physics and Astronomy, Aarhus University, 8000 Aarhus C, Denmark

[3] Max-Planck-Institut für Plasmaphysik, EURATOM Association, Boltzmannstr. 2, 85748 Garching, Germany

[4] Department of Particle Physics and Astrophysics, Weizmann Institute of Science, Rehovot 76100, Israel

E-mail: A.Wolf@mpi-hd.mpg.de

Abstract. Imaging of photofragments from molecular ions after irradiation by soft X-ray photons has been realized at the ion beam infrastructure TIFF set up at the FLASH facility. Photodissociation of the two-electron system HeH^+ at 38.7 eV revealed the electronic excitations and the charge-state ratios for the products of this process, reflecting the non-adiabatic dissociation dynamics through multiple avoided crossings among the HeH^+ Rydberg potential curves. Dissociative ionization of the protonated water molecules H_3O^+ and $H_5O_2^+$ at 90 eV revealed the main fragmentation pathways after the production of valence vacancies in these ionic species, which include a strong three-body channnel with a neutral fragment ($OH + H^+ + H^+$) in H_3O^+ photolysis and a significant two-body fragmentation channel ($H_3O^+ + H_2O^+$) in $H_5O_2^+$ photolysis. The measurements yield absolute cross sections and fragment angular distributions. Increased precision and sensitivity of the technique was realized in recent developments, creating a tool for exploring X-ray excited molecular states under highly controlled target conditions challenging detailed theoretical understanding.

PACS numbers: 33.80.-b, 36.40.Wa

1. Introduction

Charged molecules are important species in many media and often essential as carriers of chemical activity. Examples are ion chemistry in the atmosphere [1, 2], in space [3, 4, 5] where it leads to the formation of complex molecules [6, 7] in a very cold and dilute environment, or the ubiquitous role played by ions in aqueous solutions [8, 9, 10, 11], including biological systems [12]. For experimental studies of the interaction with radiation, ionic molecules and clusters in well-defined initial states constitute a special

group of targets, often only accessible using discharge sources or other dedicated ion preparation techniques. This is particularly true for a large number of protonized species, for anions, as well as for important cations that do not have isobaric neutral precursors, such as HeH^+, H_3^+, noble-gas dimer ions, and many others. X-ray absorption by neutral targets often leads to ionized molecular species as intermediate states during multi-step processes; however, such systems mostly have different conformations than the charged molecules and clusters occurring in ionized natural media.

Further appealing aspects of radiative interactions with ionic targets are the direct possibility of mass discrimination for the investigated species and the high degree of control over their kinematics before the photon interaction. In fact, the production of the target in a fast, well-controlled beam motion reveals itself as a particularly versatile tool for studies of radiation-induced molecular fragmentation, in particular by direct momentum spectroscopy of both neutral and charged dissociation products.

Interaction of monochromatic X-rays with ionic targets is experimentally still a sparsely explored area. The spatial density achievable with ionic targets is limited by the repulsive space-charge field between the particles. For experiments at synchrotron radiation sources, the best combination of high target thickness and efficient detection of photoproducts is offered by the geometry of merged ion and photon beams, which has been applied for several years to measure X-ray ionization cross sections for atomic ions [13, 14] as well as for some molecular systems [15]. However, experiments analyzing the fragmentation momenta have not been possible in this extended target geometry, which is also unfavorable for detecting the emitted photoelectrons with angular and energetic resolution.

The intense photon pulses from soft-X-ray free-electron laser (FEL) sources, as pioneered by FLASH [16], have opened the way to studies of X-ray interaction with dilute ionic targets in well-localized, point-like geometry, addressing in particular the fragmentation processes induced by X-ray absorption of molecular ions. Such molecular ion fragmentation measurements have earlier demonstrated their power in studies of the dissociation by ultraviolet laser absorption [17, 18, 19, 20] and by electron impact [21, 22], in coincidence imaging of molecular-ion fragmentation in charge exchange reactions [23, 24] and in laser fragmentation studies of molecular anions and of fast neutral molecules from anion photodetachment [25, 26] but were only recently attempted with the new high-energy photon sources.

Below we will discuss results from fast-beam fragmentation imaging using soft-X-ray photons from FLASH to excite or further ionize small molecular cations. Following an outline of the apparatus, we will present fragment momentum spectroscopy for the dissociation of HeH^+ via photoexcited Rydberg states, where the translational motion of the outgoing atoms and their charge states reflect the multistate dynamical evolution of the excited electron in the field of the dissociating core ions. In polyatomic systems, fragment spectroscopy following the photoionization of valence electrons was performed on protonated water molecules, exploring the multidimensional potential landscapes associated with valence vacancies in these systems.

2. Apparatus

The experimental scheme developed for exploring X-ray fragmentation of molecular ions at FLASH with the TIFF ion facility ("Trapped Ion Fragmentation at FLASH") [27, 28] is shown in Figure 1. The FEL beam, approximately half-way between a focusing mirror and the platform foreseen for experiments with the focused beam, is crossed by an ion beam of ∼2–8 keV kinetic energy, fast enough to let photofragments travel on in a forward cone around the ion beam direction. These cones are intersected in a cylindrically symmetric arrangement by microchannel-plate detectors used to measure the impact positions and times of the fragments and capable of analyzing fragment coincidences. In the geometry realized, angular ranges of ∼40–150 mrad and of 0–26 mrad are covered by the detectors D1 and D2, respectively, as shown in Figure 1. The typical flight times of the fragments from the interaction point to the detectors are of the order of 1–10 μs. Using delay-line readout of the pulses, impact positions and impact times are recorded for single or multiple coincident fragments, covering up to 30 FLASH pulses of a train and applying a pulse spacing of normally 5 μs.

The ion beam photofragment imaging facility TIFF implementing the described detection scheme is shown in Figure 2. It essentially runs along the monochromator beamline PG2 of FLASH and the ion–photon crossing point is situated just before the exit of this beamline towards its experimental focus. The ion beam is accelerated to a few keV for efficient beam transport as well as for fast-beam imaging into a narrow forward cone; it is transported by mostly electric deflecting and focusing elements. Mass filtering of the ions is performed by a small magnetic deflector. So far, fast-ion imaging at TIFF is performed with continuous plasma ion sources. In order to counteract the considerable vibrational and rotational excitation of ions in such sources, the option

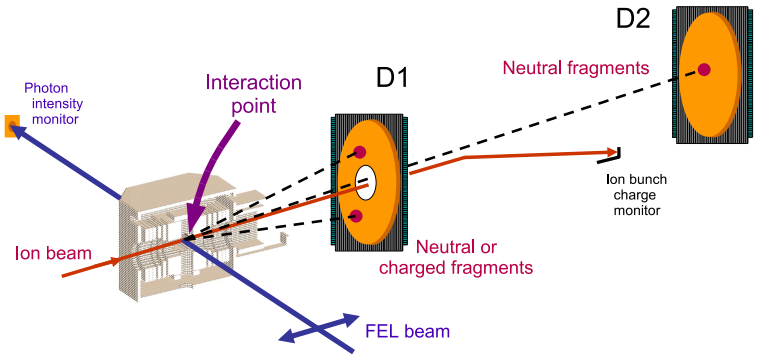

Figure 1. Scheme of the TIFF experimental arrangement for studying crossed-beam photofragmentation on molecular ion beams with kinetic energies of ∼2000–8000 eV. The microchannel-plate imaging detectors (80 mm diameter with delay-line readout) are located at distances of 0.263 m (D1) and 0.872 m (D2) from the interaction point (unless noted otherwise). The free central opening of D1 has a diameter of 16 mm. The box around the photon–ion crossing point houses biasing electrodes shaped on the basis of ion optical modeling [28]. The polarization of photons from FLASH is shown by the double arrow.

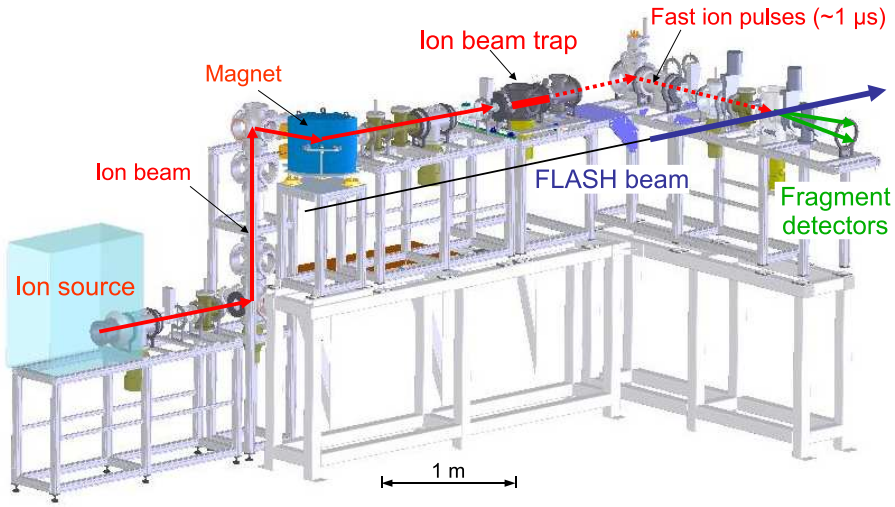

Figure 2. The TIFF ion beam facility at the PG2 beamline of FLASH. The photon–ion interaction point and the fragmentat detectors (see Figure 1) are schematically indicated. The photon beam with a diameter of ∼2 mm at the TIFF crossing point has its focus about 1.5 m downstream on the PG2 experimental platform.

has been implemented to pre-store the molecules in a fast-beam trap, where they can radiatively de-excite. For some species, substantial vibrational relaxation is possible already in the 200 ms break between the FLASH pulse trains. The pre-trapping of the ions is combined with a fast pulsing of the beam, both by emptying the trap contents by repeated pulses synchronized with a FLASH pulse train and by pulsing of a directly transported continuous ion beam. In principle, ion trapping directly in the interaction region, as demonstrated for laser multiphoton dissociation of fast molecular ions [29], offers more flexibility and efficiency; however, this technique somewhat compromises the fragment imaging and hence was not implemented in the initial experiments. In test operation, small electrostatic ion traps around the photon crossing have been shown to be operational.

The TIFF ion infrastructure was developed and tested during 2003–2005 at the Max-Planck Institute for Nuclear Physics in Heidelberg, Germany, and taken into operation at FLASH in early 2006.

3. Photodissociation of elementary molecular cations: HeH^+

Single-photon non-ionizing excitation of molecules produces a population with a well-defined total energy in high-lying potential surfaces. In photodissociation, these surfaces involve excited electrons in dissociating molecular states, in which the outcome of the fragmentation process depends on the time evolution of the system during and immediately following irradiation and can only approximately be described by adiabatic molecular potentials. Having experimental control of the electronic excitation via the photon energy and distinguishing the charge states of the fragments, studies of the fragment kinetic energy release (KER) in this process reveal both the accessible

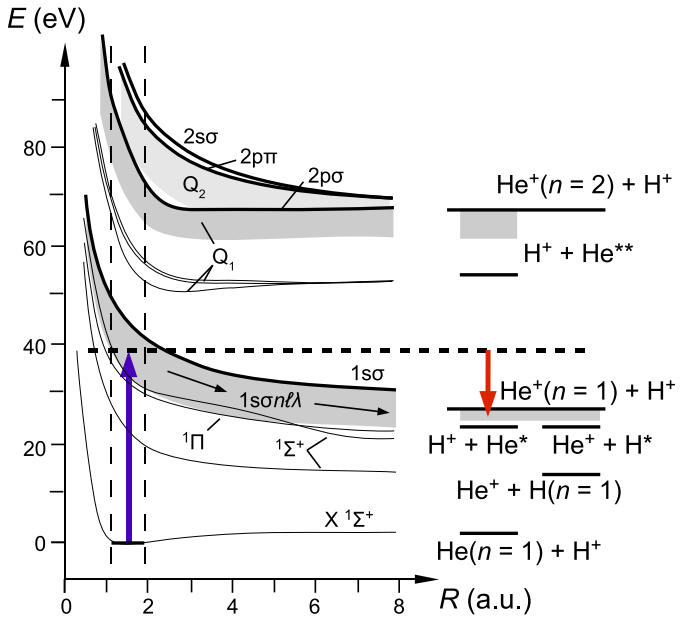

Figure 3. Potential curves of the HeH^+ ion (thin lines) of $^1\Sigma$ and $^1\Pi$ symmetry and the potentials of the one-electron system HeH^{++} [33] together with the final atomic levels. Gray areas indicate bunches of Rydberg states, while the dashed vertical lines mark the Franck-Condon zone of the photoexcitation from the initial state. The photodissociation process studied at TIFF is indicated.

electronic excitation channels within the Franck-Condon region of the initial vibrational wave function and the time evolution of the electronic state amplitudes during the dissociation. While current studies of non-adiabatic effects in the photodissociation dynamics are often devoted to heavier neutral systems and fine structure couplings [30, 20], studies on lighter molecules can more directly address the dynamics of coupled electronic and nuclear motion. This is particularly true for elementary molecular ions, where non-adiabatic coupling can also influence the charge states of the products.

Some studies on single-photon dissociation of molecular ions were performed using ultraviolet lasers [17, 18, 20]. However, even for the elementary species data on these processes are scarce, as measurements starting in the molecular ground state mostly require intense radiation pulses in the far ultraviolet and in the X-ray region. Among the light systems, the helium hydride ion HeH^+, isoelectronic to H_2, is experimentally largely unexplored regarding its photonic interactions, although it is often included in models describing systems as diverse as the chemistry in planetary nebulae [31] (where ionization by energetic photons plays an important role) or the beta decay of T_2 [32]. Fast-beam fragment imaging measurements using the intense FLASH pulses have addressed this cation as the first system.

Single-photon dissociation of HeH^+ requires at least 20 eV and, below the vertical threshold of photoionization slightly above 40 eV, produces either neutral hydrogen or neutral helium fragments, depending on the photon energy (see Figure 3). The lowest excited HeH^+ potential is clearly correlated to ground-state H fragments; it has

Σ symmetry so that the photoabsorption cross section is strongest (cosine dependence) when the photon polarization is aligned with the molecular axis. At higher energies, a band of Rydberg states is reached, which are correlated to the two fragment channels involving either a neutral hydrogen or a neutral helium atom; this is followed by dissociative photoionization at >40 eV [33]. For photodissociation, earlier calculations considered the two energetically lowest excited potentials, one of them a Π state, and found considerable photodissociation cross sections for both of them [34]. Later calculations [35] that included a large number of higher states were restricted to the Σ symmetry. In all the Rydberg band below the 1sσ potential of HeH^{++} (Figure 3) strong configuration mixing occurs [36, 37], varying with the internuclear distance as the orbitals evolve from the Li^+ united atom case to the separated atoms. The avoided crossings between the adiabatic potential energy curves imply changes of the orbital characters and hence often also swapping of the excited electron between the He and H subunits. Non-adiabatic interactions at these avoided crossings can coherently redistribute the state population during the fragmentation process over the participating electronic states and thereby considerably change the relative yield of neutral hydrogen and helium atoms as well as the excitation energies of the outgoing atoms.

The first HeH^+ photodissociation measurements with TIFF [27] were performed in 2006 at 38.7 eV photon energy, slightly below the onset of photoionization, with typical pulse energies of 10 μJ and $\sim$25 HeH^+ ions in the crossing region during a FEL pulse. Within the limited photon beam time available, fragmentation momenta of atomic He fragments could be measured for $\sim$700 signal events, deriving distributions of the kinetic energy release and of the fragmentation angle in the center-of-mass (c.m.) frame (Figure 4). As the number of usable FEL pulses would have been reduced by applying pre-storage of the ions, the HeH^+ ions were directly transferred from the plasma ion source into the interaction region and vibrationally excited states with energies up to the dissociation energy near 1.9 eV may be substantially populated.

These first measurements used the large-distance neutral detector D2 only (cf. Figure 1). The arrival times of FLASH-induced fragments and their correlation with the transverse position from the beam axis, shown in Figure 4a, revealed neutral He fragments of $\sim$10–20 eV kinetic energy release (Figure 4b) with a predominantly transverse emission direction (Figures 4c and d). Since the dissociation can be assumed to occur fast compared to molecular rotation, the fragment direction represents essentially the orientation of the molecular axis during the photoabsorption. Molecular orientations orthogonal to the laser polarization, corresponding to a Π symmetry of the excited potential, are found to dominate in the dissociation events. An absolute photodissociation cross section of 1.4 ± 0.7 MBarn is determined in which the contribution of the Σ symmetry, as deduced from the angular distributions, does not exceed 30%. The energy distribution in Figure 4b shows that neutral helium fragments are produced up to high Rydberg states with a large relative yield.

The FLASH measurements have triggered two theoretical studies [38, 39] which confirm the excited Π potential curves of HeH^+ as the dominant states for

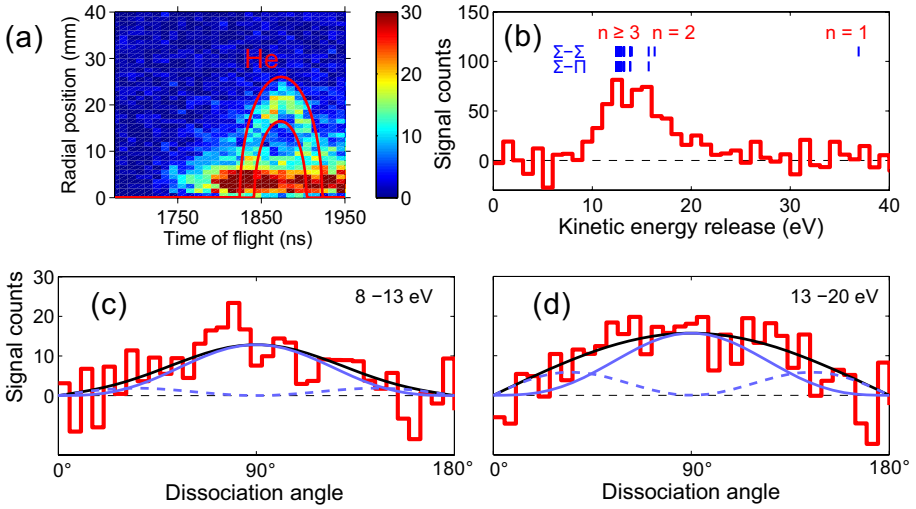

Figure 4. Neutral He photofragments from photodissociation of HeH^+ by FLASH photons of 38.7±0.6 eV observed in the first TIFF measurement [27]. Only the distant detector D2 was used at 0.987-m distance from the beam crossing point, deflecting any charged fragments before D2. In the plane of event coordinates transverse and longitudinal to the ion beam (a), the momentum sphere of He photoproducts appears on top of background neutrals from the ion beam pulse. The kinetic energy release (E_k) spectrum b and angular distributions in two parts of the E_k spectrum (c, d) were extracted. The curves in c and d indicate the fitted contributions leading into Σ levels by a broken line and the dominant contributions into Π levels, as well as the sum, by full lines. Final level energies are indicated in b. The time resolution of the readout electronics implied an additional spread of ±0.7 eV in the E_k determination in this particular measurement, which is not present in the later runs.

photodissociation into He + H^+ and both reproduce the size of the measured cross section within the experimental accuracy. Dumitriu and Saenz [38] perform calculations for 35 Σ and 25 Π states in a Born-Openheimer treatment. They compare the adiabatic and diabatic correlations for the two lowest Σ potential curves and find some, but not very substantial differences in the partial cross section for the neutral He channel between the two limiting cases. The averaging of the cross section over several excited HeH^+ vibrational levels is shown to have little influence on the photodissociation into the neutral He channel at the measurement energy of 38.7 eV. Sodoga *et al* [39] directly calculate the non-adiabatic dissociation dynamics for 12 Σ and 6 Π states. They find reasonable agreement of their result for the total cross section at the experimental photon energy applying this approach. Remarkably, their calculation shows dramatic differences between the (adiabatic) Born-Oppenheimer treatment and a full calculation of the non-adiabatic dynamics concerning in particular the Π potentials. Thus, they demonstrate that the ratio of the neutral He and neutral H channels dramatically depends on the inclusion of the radial non-adiabatic couplings as fragmentation proceeds through the lowest Π potentials, which yield the most important contribution to the cross section (Fig. 7 of Ref. [39]). The highest peak in the photodissociation cross section of HeH^+ at ∼32 eV, due to Π for >90%, is predicted to produce only the neutral

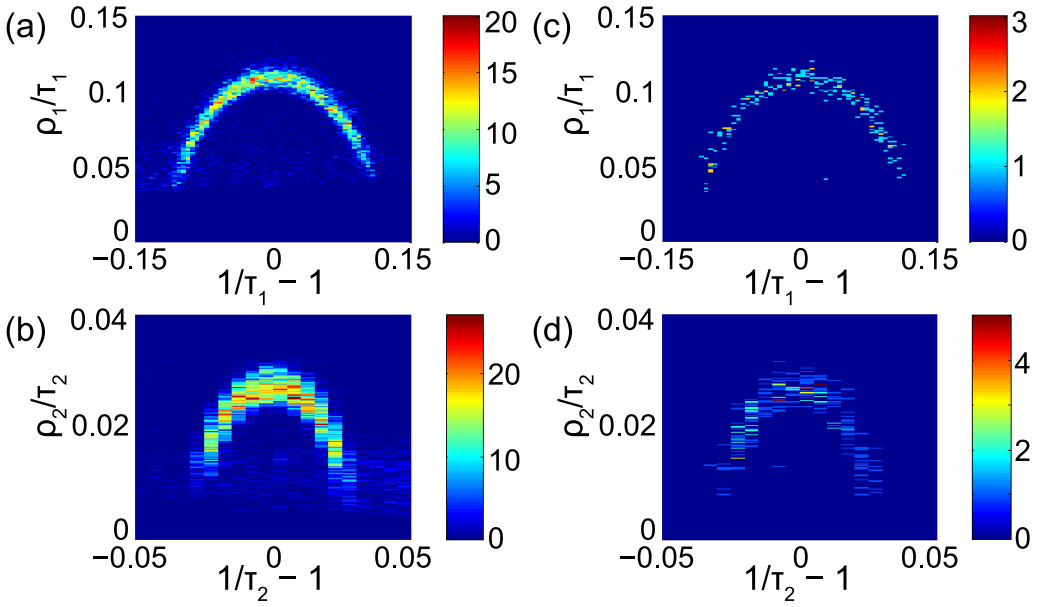

Figure 5. Coincidence imaging of photofragment pairs from HeH^+ by FLASH photons of 38.7 ± 0.6 eV from a recent TIFF measurement. The momentum spheres $\Delta p_F^{\parallel,\perp}/p_F$ are directly displayed for both, H^+ fragments on D1 (a, c) and the correlated He fragments on D2 (b, d) using the normalized detector coordinates discussed in the text (ion beam energy 4200 eV with zero bias at the beam crossing). The events shown in panels c and d were measured after storing the HeH^+ ions in the electostatic beam trap for at least 50 ms (in the range of 50–150 ms), sufficient for their radiative relaxation to essentially only $v = 0$.

H channel in the adiabatic correlation, while the full calculations predict that >30% of the excited state population are transferred into the neutral He channel by non-adiabatic interactions. At 36–45 eV, which includes the photon energy of the FLASH experiment, high-contrast oscillations of the ratio between the partial cross sections are seen in this result. Since the photon energy determines the kinetic energy in the fragmentation, this could reflect variations of the quantum phase advance between the multiple avoided crossings, underlining the importance of the non-adiabatic dynamics for the product channels in the Rydberg area studied here.

Two extensions of the HeH^+ photodissociation experiments have been realized recently at TIFF, including full kinematical analysis of the H + He^+ channel and a definition of the initial vibrational level of HeH^+ by pre-storing the ions before their transport into the interaction region. These experiments use the full set of detectors as shown in Figure 1. In addition to the neutral He channel on D2, the near detector D1 covers both H and H^+ products. Fragment imaging on this detector yields the momentum spheres for both products, which can be separated in their impact time by using a bias potential in the interaction region. Moreover, the channel H^+ + He can be accessed in full coincidence mode, strongly suppressing any background events. These results illustrate the event imaging capabilities of TIFF in two-detector mode.

Figure 5 shows the recent realization of coincidence imaging for the He + H^+

photodissociation channel of HeH^+ at 38.7 eV photon energy. Protons from the photodissociation can be detected on the near detector D1 (Figure 1) facing the interaction region. The photon-induced background on this detector could be reduced to a tolerable level, allowing even the non-coincident detection of photofragments from the ion beam, by precisely centering the FLASH beam relative to the interaction region. The fragment kinematics are suitably represented [28] in terms of the normalized event coordinates, defined relative to an undeflected and unretarded fragment present in the interaction region at the time of the FLASH pulse and moving there at the beam velocity v_I. With normalized coordinates $\rho_i = r_i/L_i$ and $\tau_i = t_i/(L_i/v_I)$ for detector i at distance L_i, the coordinates of the relative c.m. fragment momentum $\Delta\vec{p}_F = (\Delta p_F^{\parallel}, \Delta p_F^{\perp})$ are

$$\Delta p_F^{\perp}/p_F = \rho_i/\tau_i \tag{1}$$

and

$$\Delta p_F^{\parallel}/p_F = 1/\tau_i - 1 \tag{2}$$

where $p_F = m_F v_I$ is the reference momentum of a fragment with mass m_F split off from the target at velocity v_I with zero c.m. velocity. Hence, for a fragment with fixed c.m. energy of $|\Delta\vec{p}_F|^2/2m_F$ the events lie on a half-circle in the plane of the normalized event coordinates, given by

$$(\Delta p_F/p_F)^2 = (\rho_i/\tau_i)^2 + (1/\tau_i - 1)^2 \ . \tag{3}$$

The radius of an observed circle (centred at $1/\tau_i = 1$) gives the relative momentum release $\Delta p_F/p_F$ and the event density on the circle gives the distribution of the c.m. fragment emission angles. The ion beam direction and the photon polarization coincide at TIFF, ensuring angular symmetry around this common axis. While the sensitivity range of the far detector D2 of TIFF is approximately $\rho_2 < 0.03$, the near detector sees relative deflections in the range of roughly $0.04 < \rho_1 < 0.15$. Clear momentum spheres corresponding to the band of final states $He(n \geq 2) + H^+$ (Figure 3) are visible in the new coincidence data of Figure 5. Similar to the initial data, the radial size of the sphere indicates a strong contribution of higher Rydberg levels $n \geq 4$ in the photodissociation products. Further work is in progress to analyze the precise energy distributions resulting from these correlated two-body fragmentations.

Since both charged and neutral fragments of sufficient relative c.m. momentum $\Delta p_F^{\perp}/p_F$ are observed on the near detector, it is a powerful tool for analyzing the relative size of different photofragmentation channels and for HeH^+ can in particular probe the relative yields of the photofragmentation channels $H + He^+$ and $He + H^+$. Thus, it can experimentally determine the charge-state ratios for the two atomic fragments from the HeH^+ photodissociation reaction and probe the predicted significant effects on it [39] from non-adiabatic coupling between electronic potential curves during the breakup.

Separate observation of H fragments from $H + He^+$ and H^+ fragments from $He + H^+$ can be achieved by applying a bias potential over only a few millimeters around the interaction region of TIFF. Charged fragments are then, essentially longitudinally, accelerated according to their charge-to-mass ratios q_F/m_F, so that their longitudinal

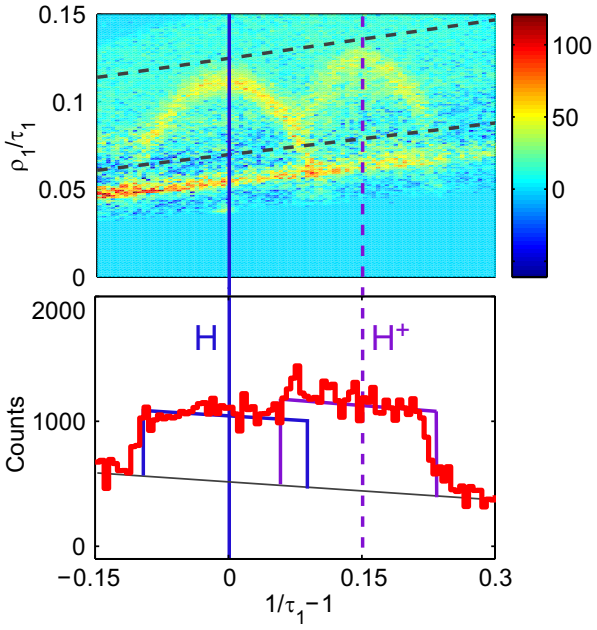

Figure 6. Photofragments from HeH^+ by FLASH photons close to 38.7 eV using the near detector D1 to observe both, the H and H^+ fragments. The momentum sphere of the product channel H^+ + He is shifted longitudinally by about +0.15 in the normalized detector coordinate $1/\tau_1$ by using a bias potential of +300 V at a beam energy of 4200 eV at the ion source. With the kinetic energy releases being very similar to each other for both channels, the projection reveals about similar strenghts for the two product charge combinations with a slight dominance (∼60/40) of the neutral He channel.

coordinate $1/\tau_1$ and, correspondingly, the center of the relative momentum sphere are shifted by a well-defined amount [28]. This is demonstrated in Figure 6 for the two competing channels of HeH^+ photodissociation. While the precise value of the branching ratio is still under analysis, it is seen that both fragment channels are present with a slight dominance of neutral helium production, He + H^+. This preliminary result is consistent with both recent calculations following the initial TIFF experiment [27] at 38.7 eV. With the feasibility of direct measurements of the product charge ratios for this elementary photodissociation reaction being demonstrated, an interesting next study of this process with TIFF could performed near 32 eV photon energy, where the cross section of the reaction assumes its highest peak. The process here is dominated in the Franck-Condon zone (Figure 3) by a single Π state that adiabatically correlates to the He^+ + H($n = 2$) channel and whose avoided crossings with other electronic states, as discussed, are predicted to redirect about a third of the dissociation events into the He + H^+ channel [39].

The radial event density on the observed fragment momentum spheres, yielding the kinetic energy release of the reaction similar to the initial result in Figure 4, is particularly sensitive to both the spectral width of the FLASH photon beam and the internal excitation of the target molecular ion. For relaxing the vibrational

distribution, TIFF uses an electrostatic mirror trap allowing repeated pulsed extraction [28] synchronized with the FLASH pulse train. In the time sequence realized in the recent test runs at TIFF, the electrostatic trap was filled ∼50-150 ms before the FLASH pulse train and was then programmed to deliver four extraction pulses of stored ions synchronized to the FLASH micropulses with a spacing of 5 μs. This emptied the trap for the light and thus relatively fast species of HeH^+, while more efficient extraction pulses will be possible with heavier molecules. The remaining photon pulses of the FLASH pulse train were overlapped with ion pulses directly from the source. Because of the small reduced mass and the high optical dipole moment of HeH^+, higher excited vibrational states in this ion spontenaously decay with radiative lifetimes of the order of 10 ms, and a Franck-Condon-type vibrational excitation is expected to be completely relaxed within <100 ms. No significant changes were seen in the shapes and radial extensions of the fragment momentum spheres; moreover, no strong influence was observed at the photon energy used (38.7 eV) on the branching ratio between the H + He^+ and He + H^+ fragment channels. The TIFF experiments used a non-monochromatized photon beam with an estimated spectral width of about ±0.5 eV, which corresponds to a few vibrational spacings in HeH^+. Thus, vibrational cooling of the ion should mainly lead to a narrowing of the Franck-Condon-region and not immediately result in the observation of sharper energetic structures in the fragment energy spectrum. Use of the monochromator in the FLASH beamline for spectral filtering, connected with a reduction of the photon flux, appears feasible in future studies with TIFF considering the improvements of both ion and photon beam intensities achieved in recent years.

In further studies of the HeH^+ photodissociation with TIFF at FLASH, it will be interesting to address different photon energies; primary interest lies in the region near 32 eV in order to investigate the product charge ratios [39] on the cross-section maximum from the lowest Π state as discussed above. Also the energy range around 60 eV is of interest, where a certain contribution from autoionizing Q_1 Rydberg states (see Figure 3) is predicted [33]. Autoionizing vibrational resonances in the lowest, bound doubly excited Q_1 state may be accessible at ∼50 eV, possibly from vibrationally excited HeH^+ states. The bound and strongly configuration-mixed excited levels of He_2^+ between 24 and 35 eV [40] are of similar interest as HeH^+ regarding the coupled electronic and nuclear quantum dynamics in small molecules, as well as the properties of the metastable bound ground state of He_2^{++}. No stable neutral target molecule offers the three-electron configuration realized in He_2^+.

4. Dissociative X-ray ionization of protonated water

A proton solvated in water is rapidly bound by a water molecule into the stable, highly symmetrical hydronium ion H_3O^+, where the proton affinity of H_2O amounts to ∼7 eV. Further structures composed of more than one water molecule around a proton are competition and the underlying molecular cluster structures are under intense research with the aim of understanding ions in aqueous environment [8, 10].

The outer valence electrons of the H_3O^+ molecule are distributed over the three OH bonds (four-fold populated 1e orbital) and over a lone-pair orbital ($3a_1$) on the oxygen atom. Considering the ionization of this molecule (see Figure 7) the electrons of the lone pair have the lowest binding energy (26.0 eV), while 31.2 eV are required for the bond electrons in 1e. The inner valence electrons are bound by 49.3 eV and found in the $2a_1$ orbital doubly occupied through, essentially, the oxygen 2s electrons (energies from Ref. [41]). For the isoelectronic system of H_2O, the states resulting from valence vacancies, corresponding to H_2O^+, have been calculated in detail [43] while much less is known about the H_3O^{++} surfaces arising from valence ionization of protonated water. Orbital geometries studied [44] for higher excited states of H_3O^+ give some information. The knowledge about valence vacancies for protonated water clusters is similarly limited, as will be discussed in Section 5.

With intense X-ray pulses, the decay kinematics following valence or core ionization becomes experimentally observable also for ionic targets. In particular, the beam geometry of TIFF gives access to a wide range of center-of-mass (c.m.) fragment emission angles in the forward cone around the incident ion direction. For the first experiment [28] after completion of the full detector system of TIFF (Figure 1) the species H_3O^+ was

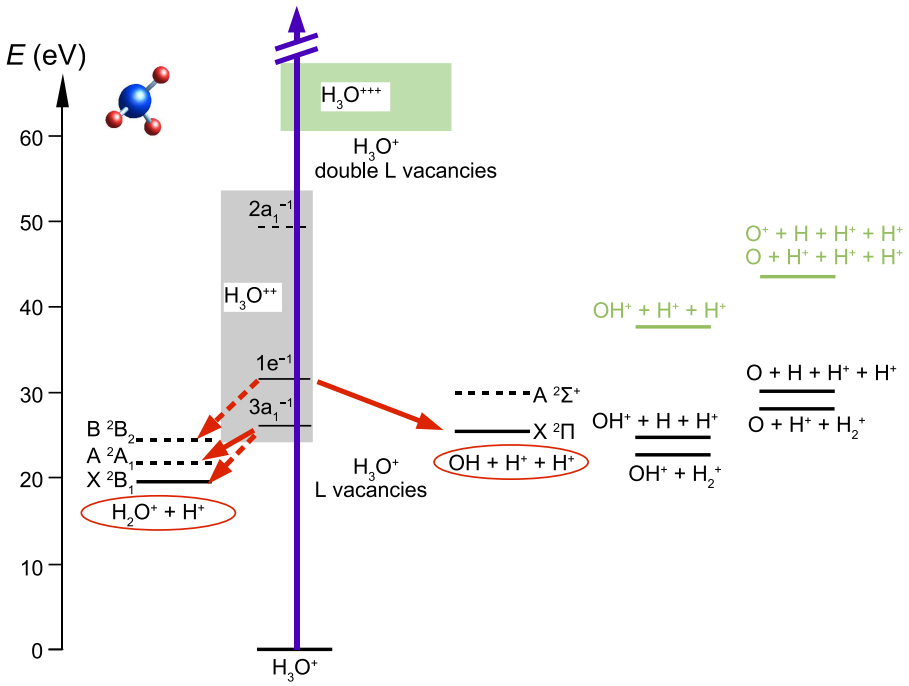

Figure 7. Orbital ionization energies [41] of H_3O^+ together with possible fragmentation energy levels reached from the corresponding valence vacancy states. The main fragmentation paths found for 90 eV photons on H_3O^+ at TIFF are shown by full downward arrows, considerably weaker channels likely to contribute some of the observed signal by broken arrows. The energy region of double valence-vacancy levels (uppermost box) is estimated with the help of Ref. [42], which also indicates that the single inner-valence excitation $2a^{-1}$ should dissolve into several energy levels around the indicated dashed line.

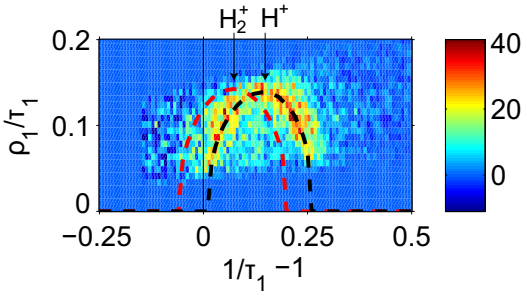

Figure 8. Photofragments from H_3O^+ by FLASH photons of 90 eV, seen on the near detector D1 of TIFF in the normalized detector coordinates [28]. With an ion beam acceleration potential of 4245 V at the source and a bias of +75 V at the beam crossing, the normalized coordinates for a fixed c.m. energy represent the momentum sphere $\Delta p_F^{\parallel,\perp}/p_F$ shifted longitudinally (in $1/\tau_1$, see marks) by +0.16 and +0.08, respectively, for charged fragments ($q_F = 1$) with masses of $m_F = 1$ and 2 amu, respectively.

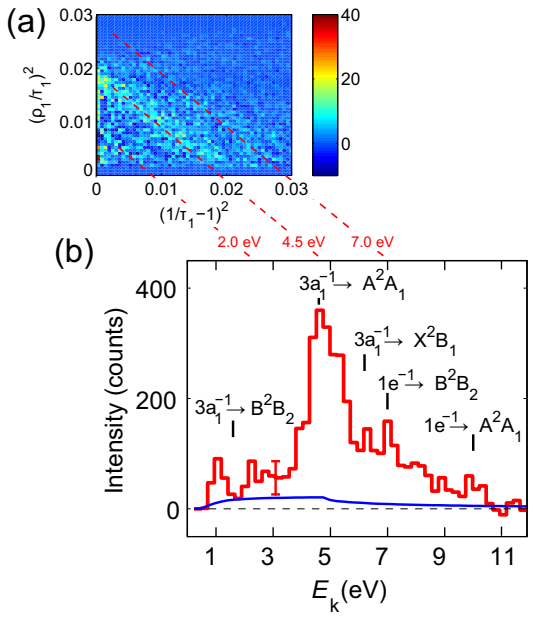

Figure 9. Correlation plot of the longitudinal and radial relative momenta $(\Delta p_F^{\parallel,\perp}/p_F)^2$ of photofragments from H_3O^+. Data from detector D1 as in Figure 8, but without a bias [28]. Diagonal structures in a represent protons (as identified through the measurement with bias) of constant c.m. energy and hence from the $H^+ + H_2O^+$ two-body breakup. The dominant line in the diagonal projection (b) corresponds to an energy release E_k of 4.5 eV, following from $(\Delta p_F/p_F)^2 = (m_{F'}/m_F)E_k/E_0$ with a beam energy $E_0 = 4245$ eV, $m_{F'} = 18$ amu, and $m_F = 1$ amu. The blue line shows the contribution expected on D1 from the three-body decay seen on D2 (Figure 10).

chosen in order to explore the X-ray photolysis of the most basic molecular structure occurring in proton hydration [8]. Neutral oxygen-containing products (masses 16–18 amu) that may arise from the dissociative ionization of H_3O^+ can be efficiently observed on the far detector (D2), while the near detector (D1) is sensitive to the proton-containing fragments (masses 1–2 amu), both charged and neutral.

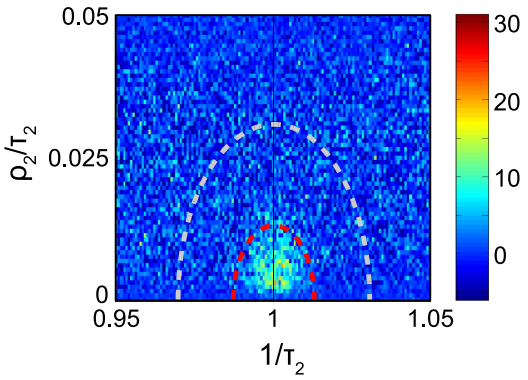

Figure 10. Neutral fragments from the dissociative ionization of H_3O^+ seen at the far detector (D2) of TIFF [27]. The red circle indicates the maximum radius of the momentum sphere for OH ions from H_3O^+ with a kinetic energy release of 6 eV; the absence of a sharp ring indicates a decay with >2 fragments. The grey circle indicates the maximum relative momentum of fragments passing through the inner bore of D1.

Two main properties of the H_3O^+ photolysis could be indentified in the fragment imaging measurements. Firstly, the fragment momenta on the near detector, when not requiring any coincidence, clearly show a dominant two-body fragmentation channel with a circular structure in the plane of the normalized fragment coordinates (see Figure 8). As described in the previous Section, the fragment charge-to-mass ratios q_F/m_F are identified by biasing the interaction region by a few percent of the ion acceleration voltage, corresponding to well-defined shifts depending on q_F/m_F. The observed shift of the circular structure identifies the dominant fragment channel as H^+, but does not support any sizable contributions from H_2^+ or from light neutrals (H, H_2). Slices of constant $(\Delta p_F/p_F)^2$, summed up in the plot of squared coordinates fulfilling Eq. (3), can then be interpreted as two-particle kinetic energy releases (Figure 9). Considering the relevant fragment energy levels relative to predicted positions [41] of valence vacancies in protonated water (Figure 7), the KER of the dominant two-body channel of ∼4.5 eV is identified as the dissociation of the $3a^{-1}$ (lone pair) vacancy level of H_3O^{++} towards the excited A^2A_1 state of the ionized water molecule H_2O^+. This electronic state has its minimum for a linear geometry ($^2\Pi_u$ [43]) and implies a vacancy in the lone-pair orbital of H_2O lying in the bending plane ($2a_1^{-1}$) [45]. The remaining events in the fragment energy release spectrum are broadly distributed with some smaller contributions likely for the channels at 7 eV (from the $1e^{-1}$ orbital) and at ∼6.5 eV (into ground-state H_2O^+); however, the dominance of the decay channel at 4.5 eV is clear, even considering the slow reduction of the geometrical detection efficiency [28] because of the outer radius of the near detector at TIFF (here above ∼5.8 eV of kinetic energy release).

Secondly, there is also substantial production of neutral O-containing fragments. This branch, mainly indicated by a signal on D2 corresponding to a broad energy release of a few eV (see Figure 10), has been analyzed in coincidence with events on D1; hence, the sample of ∼5000 events represented above is reduced to ∼740 coincidence events with D2. The momenta of the coincident fragments on both detectors are not lying on

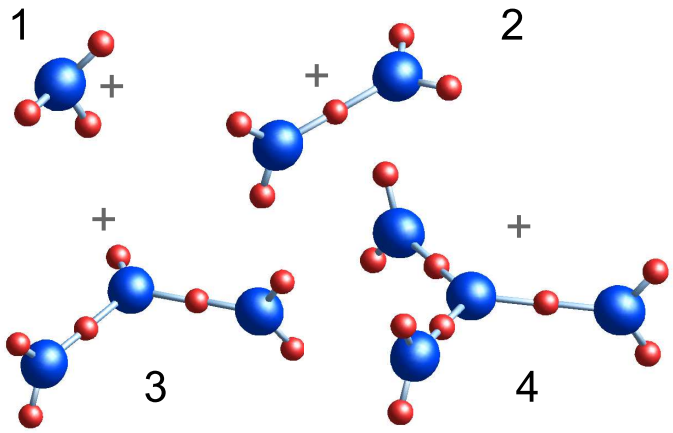

Figure 11. Shapes of the smallest protonated water clusters with $n = 1$–4 as indicated in a qualitative representation of calculated [10] structures.

a sphere, indicating the presence of more than two fragments. In addition, the average impact time with a biased interaction region indicates that the light fragments seen on D1 are protons. This finding, together with the absence of fixed KER rings in the normalized coordinates of both detectors, identifies the three-body channel OH + $2H^+$ (see Figure 7) as the origin of these events. The maximum fragment kinetic energies are of the order of 6 eV, compatible with the production of the fragment channel OH + H^+ + H^+, OH being in the electronic ground-state. The neutral fragment channel observed at TIFF has a substantial cross section measured [28] to be close to 0.4 MBarn (with an error of about 50%) and could represent up to ∼35% of all photoinduced fragmentations. The kinetic energy releases covered by D2 for possible heavy neutral fragments from H_3O^+ range up to ∼32 eV, with no important higher-energy neutral fragment channels being observed.

5. Dissociative X-ray ionization of ionic water clusters

The energy levels created by valence vacancies for protonated water clusters have been neither measured nor calculated in detail. Water clusters carrying vacancies are model systems for investigating electrostatic electron-electron interactions between distant molecular sites, notably intermolecular Coulombic decay (ICD) [46] and related processes. Recent theoretical work [42, 47] was devoted to the vacancy level energies of in small water clusters near a positive charge; here, the case of solvated Li^+ was treated in detail, and some indicative information can be derived for solvated H^+ structures [42], although the internuclear (O–H^+–O) distances in the equilibrium geometries of protonated water clusters [48] are expected to be considerably smaller when compared to the O–Li^+–O distances assumed in Ref. [42]. Experimentally, both valence vacancy levels and dissociation following photoabsorption of positive water cluster ions are essentially unexplored.

A hydrated proton can be firmly bound to a single water molecule as in H_3O^+ or at

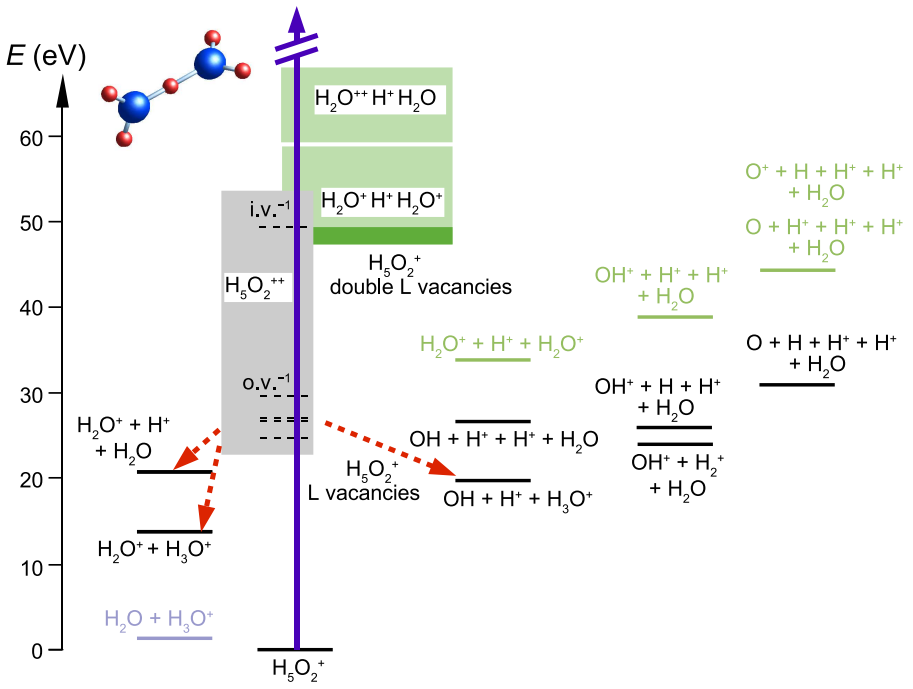

Figure 12. Valence vacancy energies of the protonated water cluster ($H_5O_2^+$) approximately indicated [42] as discussed in the text, together with possible fragmentation energy levels. Fragmentation channels compatible with the observations at TIFF are indicated by dashed arrows without implying specific outer-valence vacancy levels.

an equidistant position between two water molecules as in the $n = 2$ cluster ion $H_5O_2^+$ [11]. Other forms of binding with different nuclear spacings are found in the higher clusters, with a high degree of symmetry being restored for $n = 4$. The energy levels of X-ray produced vacancies vary with the nuclear spacings around the excess proton and are governed by varying geometrical conditions; the shifts of the electronic energies as well as the changing conformations can significantly influence the pathways of X-ray hydrolysis of these systems. Knowledge of the electronic structure and the fragmentation pathways of well-defined cationic cluster structures may be helpful in establishing X-ray absorption as an experimental tool for probing the molecular conformations in proton solvation; even fast time-dependent studies may become possible in such a scheme.

The energy levels relevant for the fragmentation of the $H_5O_2^+$ ($n = 2$) water cluster ion are illustrated in Figure 12, indicating approximate positions for the electronic energies aided by the recent theoretical work on vacancies in small water clusters around Li^+ as discussed above. In comparison to H_3O^+, there are additional alternatives for the fragmentation, and the possibility of creating vacancies at different sites (as identified by the oxygen unit) also is likely to open autoionization pathways for the valence vacancies not acessible in protonated $n = 1$ water. Thus, absorption of a single photon could lead to the emission of two electrons already in the range of inner valence excitations; below the inner valence vacancy (i.v.$^{-1}$ in Figure 12) lower two-site double-vacancy states

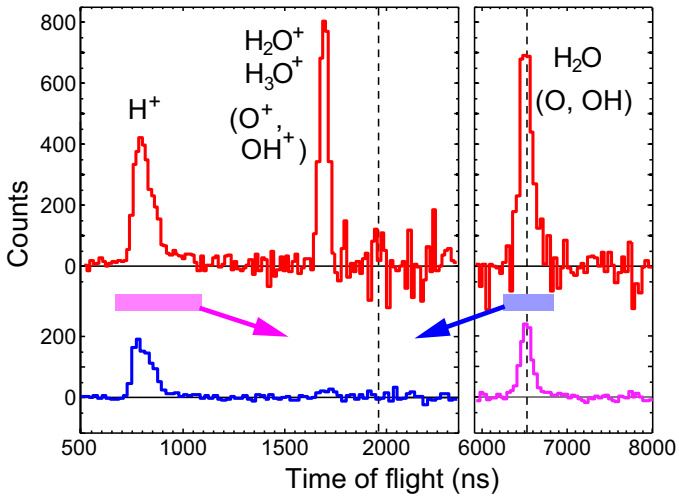

Figure 13. Fragment time-of-flight spectra (background subtracted) from photofragmentation of $H_5O_2^+$ ions at TIFF with 90 eV photons from FLASH. The laboratory ion energy is near 3440 eV in the interaction region which is biased by +700 V. Fragment times of flight are shown for detectors D1 (left) and D2 (right) and, for neutral fragments, amount to 1960 ns and 6520 ns, respectively (dashed lines). The flight times calculated with the bias for fragment ions of varying mass m_F identify the peak near 800 ns as H^+ and the one at 1700 ns as ions with m_F = 16–19 amu (adjacent masses spaced by only ∼13 ns). The upper traces show all events, while the lower traces show the time spectra for conicidences with counts from the respective other detector in the windows marked. The assigned fragments (see the text; other unlikely alternatives in brackets) are labeled.

may exist at the ground-state conformation of $H_5O_2^+$ that could serve as final states for ICD. The possible energetic opening of this mechanism is indicated schematically by the highlighted band below the i.v.$^{-1}$ levels in Figure 12, and, indeed, electronic state calculations [42] for the geometry of $Li^+(H_2O)_n$ clusters with a bare positive excess charge replacing the Li cation indicate a slightly positive energy gain for some ICD-type autoionization channels also in $H_5O_2^+$.

From the observations on neutral water [45] and on H_3O^+ at TIFF [28], X-ray absorption on a protonated water cluster can be expected to involve a strong contribution of the outer valence levels (o.v.$^{-1}$) shown indicatively in Figure 12. An experiment on the fragmentation of $H_5O_2^+$ has been performed recently at 90 eV photon energy and substantial, both charged and neutral fragmentation signals were found. At the present stage of the analysis, a tentative assignment of the products was performed by their times-of-flight from the biased interaction region, and their coincidence patterns were considered.

Figure 13 shows the time-of-flight distributions of the two detectors. Towards the near detector, charged fragments are accelerated as determined by their q_F/m_F and the observed times indicate large contributions from H^+ ions (∼700–1000 ns) and from ions of the mass range 16–19 amu (∼1600-1800 ns; a change of 1 amu in the fragment mass causes ∼13 ns of shift which so far could not be resolved). Neutrals are almost only

observed on the far detector, which qualifies them as heavy fragments (16–19 amu) of lower c.m. energy. Strong coincidences (lower traces in Figure 13) occur only between these neutrals and the H^+ products, while the heavy ionic products seem to originate from a second channel, which also has to allow them to obtain enough c.m. energy ($|\Delta\vec{p}_F|/p_F > 0.04$, corresponding to >5.5 eV in a near-equal-mass two-body decay) to reach D2. Thus, considering the channel energies in Figure 12, the H^+ and neutral signals are interpreted as signatures of the channels $H_2O^+ + H^+ + H_2O$ or $OH + H^+ + H_3O^+$, while the heavy ions observed on D1 indicate a considerable contribution of the two-body decay $H_2O^+ + H_3O^+$. Analysis of the fragment position distributions is in progress with the aim of corroborating this conclusion. Nevertheless, the results of the 90 eV photofragmentation measurements on $H_5O_2^+$ at TIFF already now suggest a large stability of the hydronium unit H_3O^+ in a sizeable fraction of the breakup events. It will be interesting to explore the branching towards this product channel, which probes the binding of the excesss proton under perturbations of the electronic structure, also for the larger protonated water clusters with even less ($n = 3$) and again higher symmetry ($n = 4$) in the trend of binding structures for increasing n.

Photofragmentation studies of these systems will strongly profit from the detection of the ionized electrons, since any possibilities of identifying the valence levels from fragmentation energies alone rapidly disappear as the systems grow, multiplying the numbers of the initial valence levels and of the available excited product states. Full electron–fragment coincidence experiments, as demonstrated for, especially, molecular anions [25] with optical laser sources, are much more demanding using high-intensity X-ray pulses mainly because of the high electron background from residual gas ionization. Moreover, a wide spectrum of electron energies is expected, in particular considering also the autoionization pathways by ICD expected to open up in the larger protonated water clusters.

X-ray photofragmentation measurements on protonated water clusters appear to offer a wide range of opportunities for augmenting the understanding of these systems also because of the tremendous ongoing progress in quantum simulation studies on ion solvation in water [9] and on the dynamics of individual water clusters [11]. Thus, very detailed theoretical simulations were recently used to elucidate the fragmentation of neutral water clusters by highly charged ions [49]. Theoretical studies of this type could be transferable to the X-ray photofragmentation of protonated water clusters, while experimental studies at TIFF afford the unique definition of the initial cluster size and possibly, together with photoelectron detection, the identification of the electronic excitation triggering the breakup dynamics.

6. Outlook

The experiments with TIFF at FLASH have demonstrated the benefit of fast charge and mass selected ion beams as targets for intense X-ray pulses from an FEL in studies of single photon absorption at a well-localized ion–photon crossing point. Fast-beam

momentum spectroscopy is achieved for the photofragments and the straightforward inclusion of neutral products in the fragment imaging gives unique possibilities for analyzing the underlying fragmentation dynamics, such as coincidence imaging of neutral and charged products. Thus, the experiments not only give access to ionic molecular conformations that cannot be realized with neutral, high-density targets, but also enhance the precision at which X-ray induced molecular fragmentation dynamics can be investigated.

The initial studies reported here point to a large number of extensions regarding both the systems to address and the surrounding detection techniques, some of which were mentioned above. Fast-beam coincidence momentum spectroscopy, possibly combined with electron detection, would also be attractive for pump–probe studies, once the focusing of both beams can be increased to the small sizes required for a high excitation probability of the target in the photon field. While this would emphasize the short-pulse-length frontier of the FEL development, and probably be mainly devoted to photoionization, molecular photodissociation measurements would particularly profit from the spectral purity of seeded photon pulses. This would help in probing metastable resonances in the dissociation as well as the propagation of quantum state amplitudes on coupled molecular potential surfaces, as discussed for HeH^+, where the relative phases for possible quantum interferences will vary as a function of the initial energy of the system.

Thus, for studying the dynamics induced by outer and inner valence electron excitation in molecular systems, fast-beam momentum spectroscopy on the basis of the TIFF developments calls for powerful and highly available, seeded FEL sources in the 25–100 eV range. On the other hand, these studies can be extended to inner shell vacancies in the molecular systems by using intense high-energy FEL sources, such as LCLS, SPring-8, and XFEL. It will be challenging to keep similar excitation probabilities of the ions as at FLASH at these higher photon energies, using stronger beam focusing at the photon–ion crossing point or developing new methods with a collinear interaction zone.

Acknowledgement

The funding of the project by the Max-Planck-Institut für Kernphysik, the Max-Planck Initiative DESY FEL (MIDFEL) and the Max-Planck Advanced Study Group at the Center for Free Electron Laser Science (CFEL) is gratefully acknowledged. Thanks are due to J. Ullrich, D. Schwalm and D. Zajfman for the continuous support, to M. Martins, S. Klumpp, R. Treusch, N. Guerassimova, S. Düsterer, and to the scientific [16] and technical team of FLASH for the assistance in the setup and beamtimes, to J. Feldhaus and J. R. Schneider for assistance during the project planning, to M. Rappaport for support in the design of the ion trap, and to X. Urbain and H. Helm for help during the early design and setup phase. H.B.P. acknowledges support from the Lundbeck Foundation, and O.H. support from the German-Israeli Foundation GIF.

References

[1] Siefermann K R and Abel B 2010 *Science* **327** 280–281
[2] Relph R A, Guasco T L, Elliott B M, Kamrath M Z, McCoy A B, Steele R P, Schofield D P, Jordan K D, Viggiano A A, Ferguson E E and Johnson M A 2010 *Science* **327** 308–312
[3] Herbst E 2001 *Chem. Soc. Reviews* **30** 168–176
[4] Petrie S and Bohme D K 2007 *Mass Spectrom. Reviews* **26** 258–280
[5] Sternberg A and Dalgarno A 1995 *Astrophys. J. Suppl. Ser.* **99** 565–607
[6] Woodall J, Agúndez M, Markwick-Kemper A J and Millar T J 2007 *Astron. Astrophys.* **466** 1197–1204
[7] Vasyunin A, Semenov D, Wakelam V, Herbst E and Sobolev A 2008 *Astrophys. J.* **672** 629–641
[8] Marx D, Tuckerman M E, Hutter J and Parrinello M 1999 *Nature* **397** 601–604
[9] Kornyshev A A, Kuznetsov A M, Spohr E and Ulstrup J 2003 *J. Phys. Chem. B* **107** 3351–3366
[10] Headrick J M, Diken E G, Walters R S, Hammer N I, Christie R A, Cui J, Myshakin E M, Duncan M A, Johnson M A and Jordan K D 2005 *Science* **308** 1765–1769
[11] Niedner-Schatteburg G 2008 *Angew. Chem. Int. Ed.* **47** 1008–1011
[12] Wolf S, Freier E and Gerwert K 2008 *Chem. Phys. Chem.* **9** 2772–2778
[13] Kjeldsen H 2006 *J. Phys. B: At. Mol. Opt. Phys.* **39** R325–R377
[14] Schippers S, Müller A, Ricz S, Bannister M, Dunn G, Schlachter A, Hinojosa G, Cisneros C, Aguilar A, Covington A, Gharaibeh M and Phaneuf R 2003 *Phys. Rev. A* **67** 032702
[15] Müller A, Schippers S, Habibi M, Esteves D, Wang J, Phaneuf R, Kilcoyne A, Aguilar A and Dunsch L 2008 *Phys. Rev. Lett.* **101** 133001
[16] Ackermann W *et al* 2007 *Nat. Phot.* **1** 336–342
[17] von Busch F and Dunn G H 1972 *Phys. Rev. A* **5** 1726–1743
[18] Helm H and Cosby P C 1987 *J. Chem. Phys.* **86** 6813–6822
[19] Sarre P J, Walmsley J M, Whitham C J and Duxbury G 1988 *Phil. Trans. Roy. Soc. London Ser. A* **324** 233–246
[20] Hechtfischer U, Amitay Z, Forck P, Lange M, Linkemann J, Schmitt M, Schramm U, Schwalm D, Wester R, Zajfman D and Wolf A 1998 *Phys. Rev. Lett.* **80** 2809–2812
[21] Abdellahi El Ghazaly M O, Jureta J, Urbain X and Defrance P 2004 *J. Phys. B: At. Mol. Opt. Phys.* **37** 2467–2483
[22] Zajfman D, Amitay Z, Broude C, Forck P, Seidel B, Grieser M, Habs D, Schwalm D and Wolf A 1995 *Phys. Rev. Lett.* **75** 814–817
[23] de Bruijn D P, Neuteboom J, Sidis V and Los J 1984 *Chem. Phys.* **85** 215–231
[24] van der Zande W J, Koot W, de Bruijn D P and Kubach C 1986 *Phys. Rev. Lett.* **57** 1219–1222
[25] Continetti R E 2001 *Ann. Rev. Phys. Chem.* **52** 165–192
[26] Continetti R E, Cyr D R, Metz R B and Neumark D M 1991 *Chemical Physics Letters* **182** 406–411
[27] Pedersen H B, Altevogt S, Jordon-Thaden B, Heber O, Rappaport M L, Schwalm D, Ullrich J, Zajfman D, Treusch R, Guerassimova N, Martins M, Hoeft J T, Wellhöfer M and Wolf A 2007 *Phys. Rev. Lett.* **98** 223202
[28] Pedersen H B, Altevogt S, Jordon-Thaden B, Heber O, Lammich L, Rappaport M L, Schwalm D, Ullrich J, Zajfman D, Treusch R, Guerassimova N, Martins M and Wolf A 2009 *Phys. Rev. A* **80** 012707
[29] Orr P A, Williams I D, Greenwood J B, Turcu I C E, Bryan W A, Pedregosa-Gutierrez J and Walter C W 2007 *Phys. Rev. Lett.* **98** 163001
[30] Brown A 2007 *Int. J. Quantum Chem.* **107** 2665–2671
[31] Cecchi-Pestellini C and Dalgarno A 1993 *Astrophys. J.* **413** 611–618
[32] Jonsell S, Saenz A and Froelich P 1999 *Phys. Rev. C* **60** 034601
[33] Fernandez J and Martin F 2007 *J. Phys. B: At. Mol. Opt. Phys.* **40** 2471–2480
[34] Basu D and Barua A K 1984 *J. Phys. B: At. Mol. Opt. Phys.* **17** 1537–1545
[35] Saenz A 2003 *Phys. Rev. A* **67** 033409

[36] Green T A, Michels H H, Browne J C and Madsen M M 1974 *J. Chem. Phys.* **61** 5186–5199
[37] Green T A, Michels H H and Browne J C 1976 *J. Chem. Phys.* **64** 3951–3956
[38] Dumitriu I and Saenz A 2009 *J. Phys. B: At. Mol. Opt. Phys.* **42** 165101
[39] Sodoga K, Loreau J, Lauvergnat D, Justum Y, Vaeck N and Desouter-Lecomte M 2009 *Phys. Rev. A* **80** 033417
[40] Bawagan A D O and Davidson E R 1997 *Chem. Phys. Lett.* **266** 499–506
[41] Raffenetti R C, Preston H J T and Kaufman J J 1977 *Chem. Phys. Lett.* **46** 513–518
[42] Müller I B, Cederbaum L S and Tarantelli F 2004 *J. Phys. Chem. A* **108** 5831–5844
[43] Schneider F, Di Giacomo F and Gianturco F A 1996 *J. Chem. Phys.* **105** 7560–7568
[44] Di Giacomo F, Gianturco F A, Raganelli F and Schneider F 1994 *J. Chem. Phys.* **101** 3952–3961
[45] Karlsson L, Mattsson L, Jadrny R, Albridge R G, Pinchas S, Bergmark T and Siegbahn K 1975 *J. Chem. Phys.* **62** 4745–4752
[46] Cederbaum L, Zobeley J and Tarantelli F 1997 *Phys. Rev. Lett.* **79** 4778–4781
[47] Müller I B and Cederbaum L S 2005 *J. Chem. Phys.* **122** 094305
[48] Yeh L I, Okumura M, Myers J D, Price J M and Lee Y T 1989 *J. Chem. Phys.* **91** 7319–7330
[49] Adoui L, Cassimi A, Gervais B, Grandin J, Guillaume L, Maisonny R, Legendre S, Tarisien M, Lopez-Tarifa P, Politis M, du Penhoat M H, Vuilleumier R, Gaigeot M, Tavernelli I, Alcami M and Martin F 2009 *J. Phys. B: At. Mol. Opt. Phys.* **42** 075101